

Signal analysis of axial and flexural behavior in high strain dynamic pile testing

Malek Allani & Alain Holeyman

Université Catholique de Louvain, Belgium

ABSTRACT: It is difficult to control the co-axiality of the ram mass with respect to the neutral axis of the pile in dynamic pile testing. This results in non axial effects on pile response, as illustrated by presented case histories (Tessengerlo and Limelette sites) of eccentric impacts on piles. Geotechnical site characterization of both sites is first presented. We then focus on axial signal analysis to represent the main relationship between measured quantities (drop heights, settlements...). Flexural pile behavior is also studied to estimate the flexural energy and to understand the effects of the ram misalignment on measurements. Finally, we discuss the effect of eccentricity on dynamic bearing capacity using the Case method.

1 INTRODUCTION

Pile load testing has become nowadays a routine technique for deep foundation quality control. High strain dynamic pile testing consists in the measurement of pile strain and acceleration at the pile head under impacts of large weights. Pile strains and accelerations are measured with strain transducers and accelerometers, respectively. The objectives of such testing are the definition of bearing capacity and the estimate of possible deformation under working load. A 1-D longitudinal approach is often used to model the pile/soil system (Smith 1960; Holeyman 1984) while several methods of signal processing are applied to measured signals (strain and acceleration at pile head) with a view to fine-tune computed signals (Case method, NUSUMS, CAPWAP...). However, it is worth noting that Dynamic Loading Tests (DLTs) still include some limitations even though high technology and sophisticated interpretation are used during measurement and for inverse analysis. An important uncertainty or difficulty we may find in a DLT is the complex combination of compressive, tensile and also bending effects that may induce potentially damaging stresses and signal miss matching. Reconciliation of the stress wave measurements with theory may be achieved by considering non axial effects in DLTs. In fact, not only compressive waves but also flexural oscillation and pile whipping can be generated by the ram impact. Poskitt (1992), Holeyman (2000) and Charue (2004), indicate that eccentricity of the mass ram is often observed in DLTs while extreme conditions may be reached in pile driving.

Case histories of pile dynamic testing under eccentric impact are presented. First we present the Limelette and Tessengerlo site geotechnical characterization and the experimental procedure. Then, axial and flexural signal analysis is performed with a focus on transferred energy to the pile and ram-pile misalignment effects.

2 GEOTECHNICAL CHARACTERISATION AND EXPERIMENTAL PROCEDURE

2.1 Geotechnical sites description

The CPT results presented in figures 1 and 2, show typical CPT profiles for the Limelette and Tessenderlo sites, both located in Belgium.

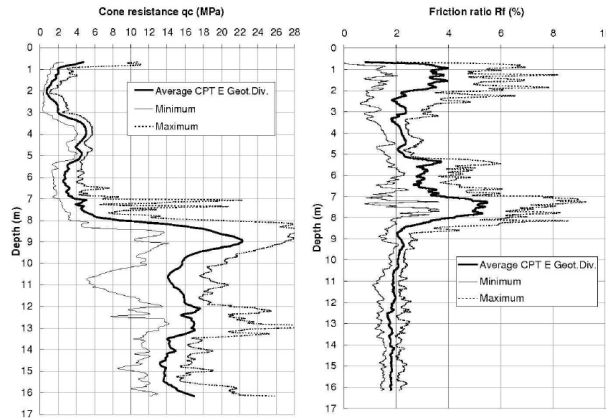


Figure 1: Mean, min and max q_c and R_f values for the dynamic test field of limelette (after VanAlboom, G and Whenham, V, 2003)

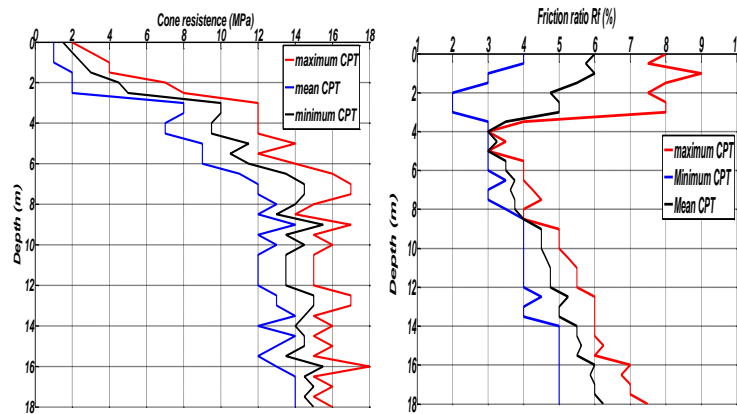


Figure2: Mean q_c and R_f values for the dynamic test field of Tessenderlo.

These CPT present the following stratigraphy: 8 m thickness of silt layer over Brussellian sand layer at Limelette and compact sandy silt in the top 6 m over silt to clayey sand layer at Tessenderlo.

2.2 Experimental procedure and data reduction

Dynamic impacts on piles were generated by a Dynamic Loading Test Module. The system, called FondyTest, has been developed at the Department of Civil and Environmental Engineering of UCL. It consists in a 4 tons ram mass with an adjustable drop height, easily transportable to the field (fig.3). The eccentricity of impact may also be controlled thanks to an automatic air cushion actuation. The actual eccentricity imposed in each blow might also be verified manually in the field.

In the Limelette site, a driven precast prestressed square concrete pile with $a = 35$ cm side and 9.5 m length was tested.

A continuous flight auger pile, with large hollow stem of diameter $2r = 60$ cm and about 15.5 m long was tested at the Tessenderlo site.



Figure 3: DLTM transported in field Figure 4 : strain gauge and accelerometers on pile head

Figures 3 and 4 present the geometrical configuration of transducers for both sites with reference to pile axes, where showing on the four sides of the piles heads uniaxial piezoelectric accelerometers (Acc) and strain gauges (Sg) were mounted.

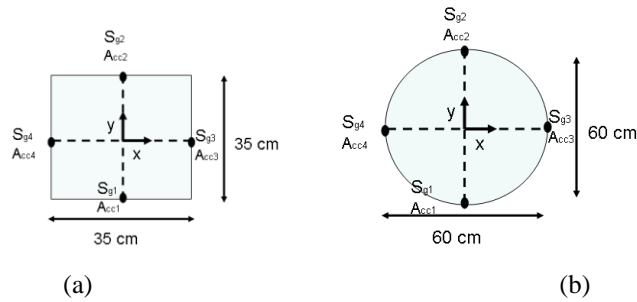


Figure 5: Sensors disposition at pile head for (a) Limelette and (b) Tessenderlo sites

Form measured acceleration, one can obtain by integration the velocity and displacement at the pile head. Unfortunately, this is not an easy task as it seems because of environmental signal noise, parasitic errors and offsetting integration problems that might affect the integration process. For noise elimination, a non-causal filtering (Butterworth type, 6th order with 1.5 kHz cutoff frequency) was used and a corrective acceleration and velocity was incorporated in real signals to eliminate integration offset. We have used PCB353B04 (500g) and PCB353M231 (5000g) accelerometer type to avoid traducers saturation based on maximum acceleration assessments. We also have considered high sampling frequencies at both sites to confirm Nyquist criteria; 20 kHz and 75 kHz for the site of Limelette and Tessenderlo respectively.

For the calculation of applied force F , we used the formula: $F = EA_p \varepsilon_{mean}$ where E : is the pile young modulus, A_p pile cross section and $\varepsilon_{mean} = \frac{\varepsilon_1 + \varepsilon_2}{2}$ is the mean measured strain within a longitudinal plane (either x or y).

Table 1, summarizes the sequential pile loading in both sites. We have to note that only the eccentricity about the x-axis direction (cf. Fig 5) is considered in the whole analysis.

Blow number	Site			
	Limelette		Tessenderlo	
	Drop height (cm)	Eccentricity(mm)	Drop height (cm)	Eccentricity(mm)
1	30	0	40	0
2	40	0	70	0
3	60	-20	110	0
4	40	-20	40	0
5	80	-20	40	37
6	80	-40	70	37
7	120	-32	40	62
8	120	-32	40	37
9	80	-29	70	37
10	80	-31	40	55
11	160	-31		
12	40	-3		
13	40	-40		
14	40	-34		

Table 1: Summary of sequential pile loading for both sites.

3 SIGNAL ANALYSIS IN COMPRESSION

3.1 Axial analysis observations

In the very first moments of the impact, measured force and velocity times the pile impedance are superposed as functions of time (fig.6). When the peak force F_{max} is compared to the peak velocity V_{max} , the trend observed (fig7) must reflect the nominal impedance of the pile I . The latter is equivalent to a dashpot factor modelling the behaviour of a semi-infinite pile subjected to

an imposed velocity at its head. We have $I = \frac{EA_p}{c} = \rho_{pile}cA_p$ where ρ_{pile} is the pile

volumetric mass and $c = \sqrt{\frac{E}{\rho_{pile}}}$ is the bar wave propagation velocity.

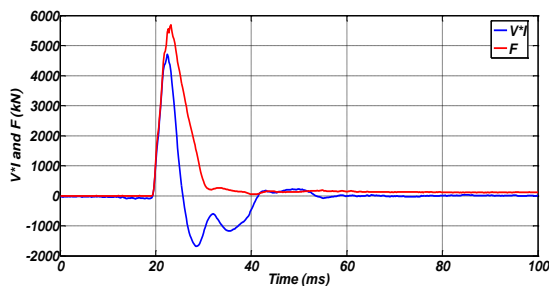


Figure 6: F and V*I traces for Tessenderlo site

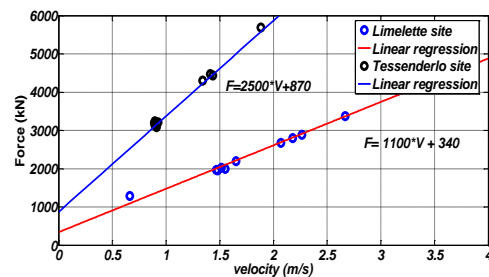


Figure 7: F_{max} and V_{max} Regression

Figures 8 and 9 present the velocity at pile head for both sites. The traces of velocities confirm the increase of the peak velocity with the drop height and a second peak is also observed

after a duration Δt which is connected to the return of the wave after reflexion on the base. Thus, the pile length L might be calculated using the relation: $\Delta t = \frac{2L}{c}$, with L =pile length.

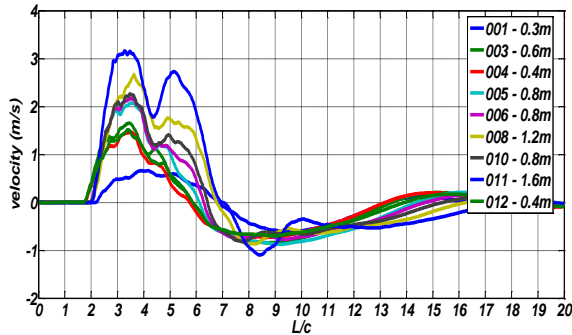


Figure 8: Velocity traces for Limelette site

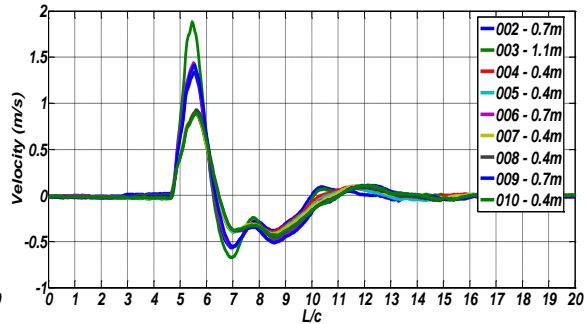


Figure 9: Velocity traces for Tessenderelo site

3.2 Axial modeling

It is worthy noting that for the same drop height (which means same ram impact velocity V_i), the pile maximum velocity V_{max} is different for both sites. In fact, since the pile impedance is evaluated (fig 8), one can model the pile head subjected an impact velocity v_i by a dashpot with a damping factor equal to the pile impedance. The one dimensional formulation of the phenomenon according to Holeyman (1992) is presented in figure 10, where M is the mass ram and K is the cushion stiffness.

Using the one-dimensional formulation, we conclude that the ratio velocity is a function of the ratio $\frac{\omega_n}{\alpha} = \frac{2I}{\sqrt{KM}}$ were $\alpha = \frac{K}{2I}$ and $\omega_n = \sqrt{\frac{K}{M}}$. However the duration of the velocity is a function of ω_n (fig.11).

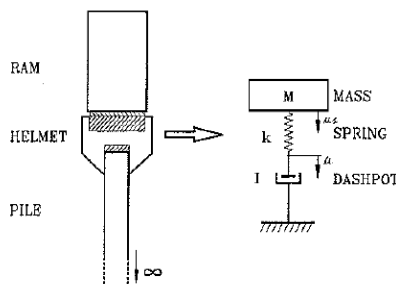


Figure 10: 1-D axial formulation (after Holeyman(1992))

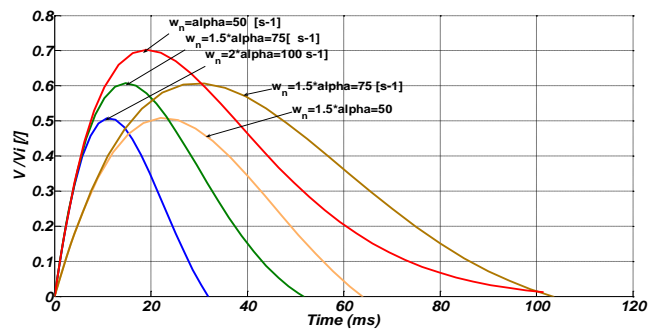


Figure 11: V_{max} / V_i ratio for different values of ω_n and α

For wave impacts of very long duration, the pile mechanical behavior should be enhanced by a spring parallel to the dashpot representing the pile equivalent static behavior.

Using the appropriate contours (fig 12), the velocity ratio is obtained knowing the values of the cushion stiffness and the ram mass. Thus, maximum force transmitted to the pile is calculated (velocity times impedance) and concrete damaging might be prevented by specifying the maximum strain range using the relation: $\epsilon_{max} = \frac{V_{max}}{c}$

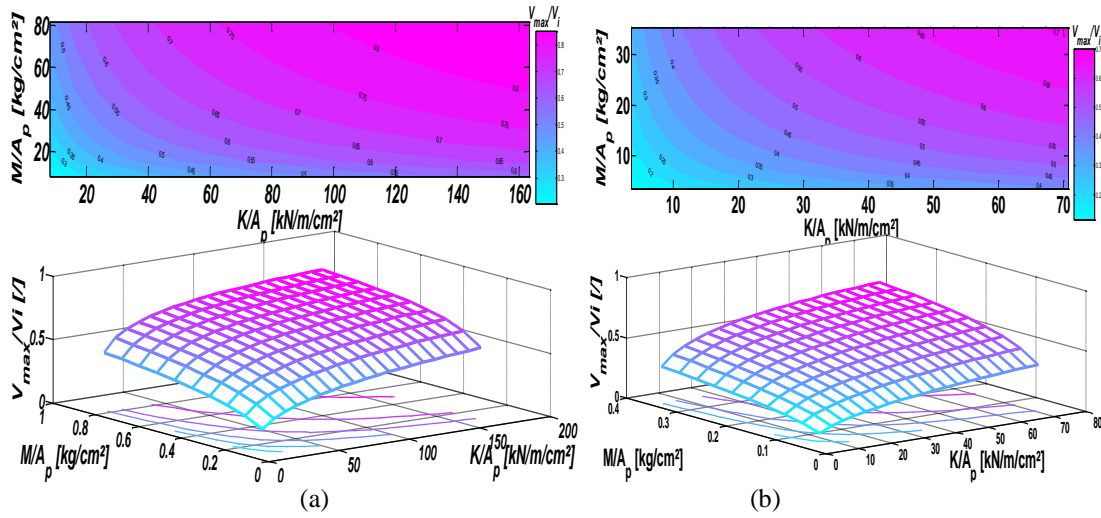


Figure 12 : V_{\max} / V_i ($L = \infty$) asunction of ram mass and cushion stiffness ratios for (a) Limelette (b) and Tessengerlo sites for $H=40$ cm.

Considering now displacement signal for both sites (Fig 13 and 14), we remark that at the Limelette site the settlement is quickly damped with no subsequent oscillation after the first loading.

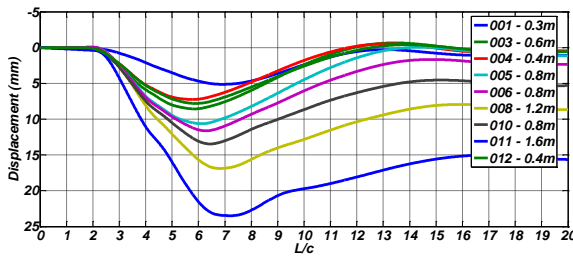


Figure 13: Displacement traces (Limelette)

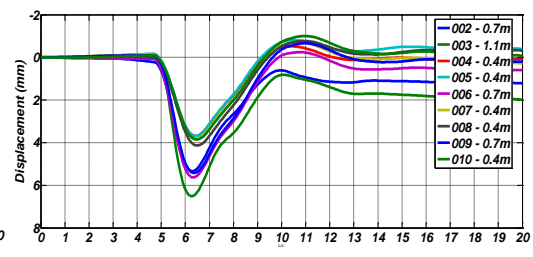


Figure 14: Displacement traces (Tessengerlo)

3.3 Axial Energy Transfer

The axial energy transmitted to the pile is called ‘Enthru’ energy. It is defined as the integration of the product of both force and velocity signals until the end of impact t_f :

$$Enthru = \int_0^{t_f} F(t)V(t)dt$$

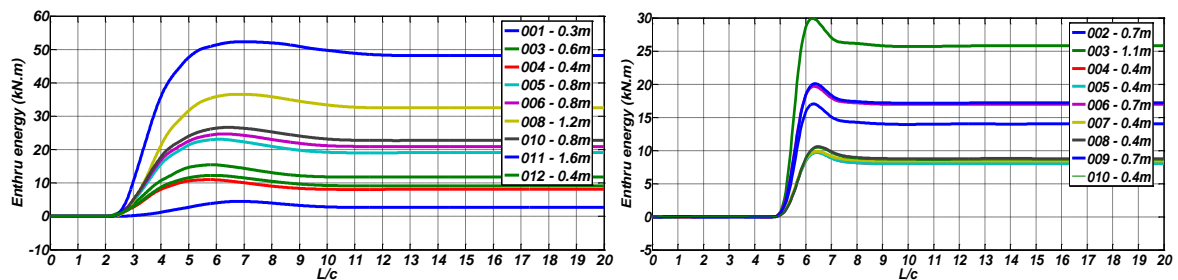


Figure 15: Enthru energy trace for (a) Limelette and (b) Tessengerlo site

This term reflects the performance of a hammer and driving system in pile driving. Figures 11 and 12 show the traces for the ‘Enthru’ energy for both sites. Similarly to the previous

reasoning of V_{\max} / V_i ratio, the transferred energy is higher for the Limelette site, for the same initial velocity impact.

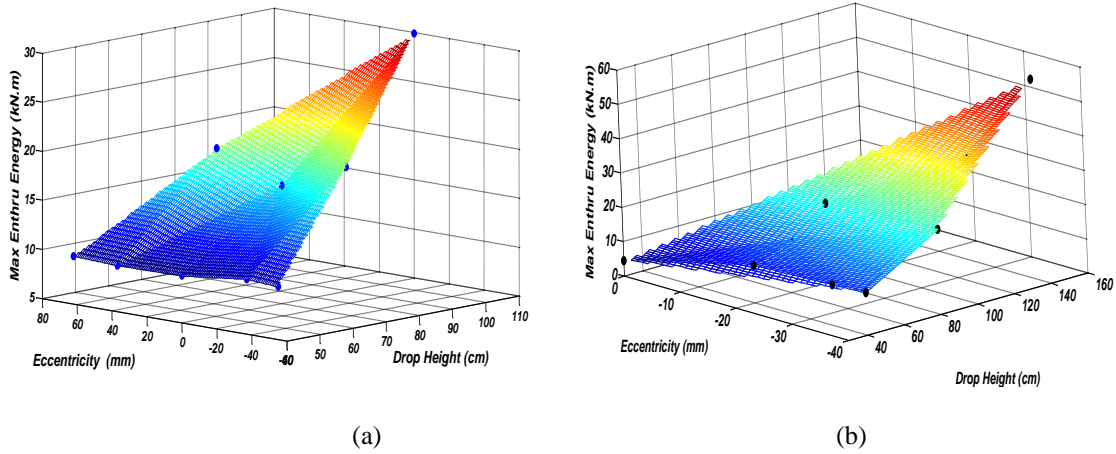


Figure 16: Maximum Enthru energy in function of drop height and eccentricity for (a) Tessenderlo and (b) Limelette sites.

To investigate the effect of the eccentricity on the maximum ‘Enthru’ energy, figures 12(a and b) show the evolution of the maximum ‘Enthru’ energy as a function of the imposed height drop and eccentricity. Unexpectedly, the maximum ‘Enthru’ energy seems to increase with the imposed eccentricity. Although several explanations can be offered, we believe that the horizontal pressure on the pile wall was not uniform around the pile perimeter. Thus, flexure of the pile produces an enlarged cavity (oval and squarish cavities trend of the cross section pile in the site of Tessenderlo and Limelette respectively) along which the pile shaft travels and energy transmission becomes higher.

4 FLEXURAL SIGNAL ANALYSIS

The bending moment M about the x-direction for both sites was calculated based on the strain gauges diametrically opposed ε_2 and ε_1 on the pile head section. Bernoulli assumptions lead to

$$M = \frac{Ea^3}{12}(\varepsilon_2 - \varepsilon_1) \text{ and } M = \frac{E\pi r^3}{8}(\varepsilon_2 - \varepsilon_1) \text{ for a square and circular cross section respectively.}$$

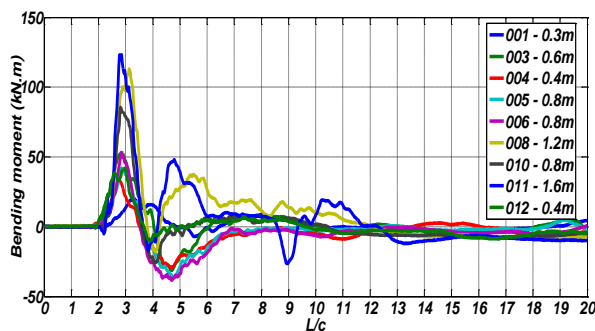


Figure 18: Bending moment for Limelette site

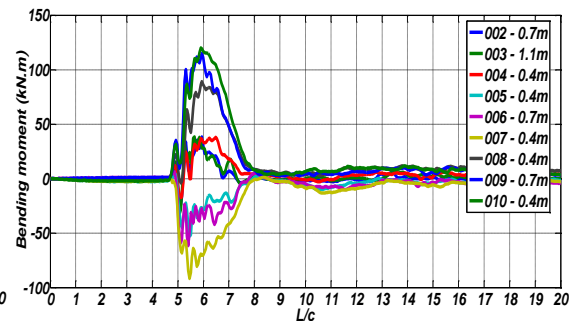


Figure 17: Bending moment for Tessenderlo site

Large bending moments (more than 100 kN.m) are observed for both sites even though limited eccentricities are imposed (figs.17 and 18). Further, the dependency of the bending moment to the eccentricity is more pronounced than to the drop height (Fig 19).

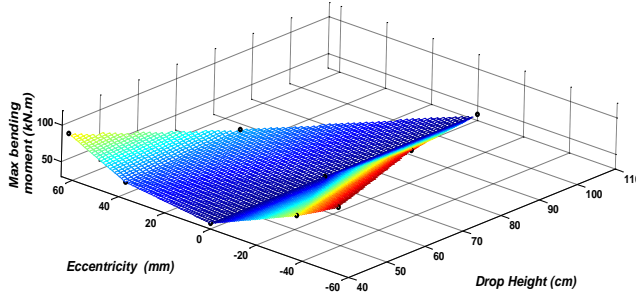


Figure 19: Max bending moment vs. eccentricity site and drop height (Tessednerlo site)

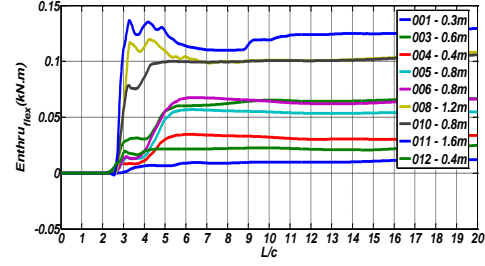


Figure 20: 'Enthru_{flex}' traces for Limelette

By analogy with axial analysis we estimate the flexural transmitted energy to pile using the relation: $Enthru_{flex} = \int_0^{t_f} M(t)\dot{\theta}(t)dt$; Where $\dot{\theta}$ is the pile head cross section rotation velocity.

The 'Enthru_{flex}' signal represented in the figure 20, is quite similar to the 'Enthru' energy. However, the ratio of the 'Enthru' axial to the 'Enthru_{flex}' is very high.

5 CASE METHOD AND DYNAMIC BEARING CAPACITY

5.1 Case method

As already explained, pile impedance represents the proportionality between force and velocity for a free semi-infinite pile where no soil interaction is considered. However, soil presence influences upward and downward force and velocity. The case method (Goble et al 1975), is based on the difference between signals of a free pile and the real situation. Assuming total mobilisation of shaft and base soil resistance in the case method, signal processing in high strain dynamic pile testing can lead to the evaluation of total resistance. According the latter assumption, rigid-plastic behaviour at the pile shaft and base is considered. Validity of this assumption especially for base modelling is discussed in Holeyman (1992) and Charue (2004). Figure 21 shows the path of a short incident wave and its interactions with the soil at depth z^* and in the pile toe at depth L . Since the reflected upward compressive wave is related to the mobilised skin friction R_f , this latter can be evaluated as: $Q_f(z^*) = \int_0^{z^*=ct} R_f = 2F^\uparrow = F - IV$. The dynamic base resistance expression is:

$Q_B = \frac{1}{2}[F(t^+) + IV(t^+)] - \frac{1}{2}[F(t^+ + \frac{2L}{c}) - IV(t^+ + \frac{2L}{c})]$; where t^+ is the time selected to obtain the maximum value of Q_B within the interval: $2L/c < t^+ < 4L/c$.

The Case method leads to a combination of shaft and base dynamic resistance to evaluate the total soil resistance based on the assumption of rigid-plastic behaviour of all terms contributing to the resistance :

$$R_{dyn_case} = \frac{1}{2}[F(t^+) + F(t^+ + \frac{2L}{c})] + I[V(t^+) - IV(t^+ + \frac{2L}{c})]$$

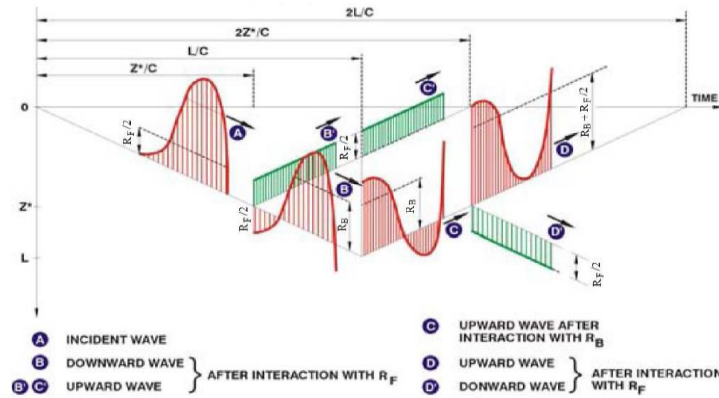


Figure 21: Sets of waves in dynamically loaded pile (Holeyman, 1992)

5.2 Case resistance analysis

Figures 22.a and 22.b show the dependence of the dynamic shaft and base resistances to the drop height and to the eccentricity. The eccentricity seems to have no effects on the shaft dynamic resistance however the dynamic base resistance seems to increase with eccentric impacts. Therefore, care must be taken when dealing with bearing capacity estimation even though ‘ $E_{thru_{flex}}$ ’ energy is negligible comparing to ‘ E_{thru} ’ energy. In fact, figure 24.b shows the dynamic resistance using the Case method in function of the drop height and eccentricity. The dynamic soil resistance increases with the drop height, however a dispersion of the dynamic resistance for the same drop height is observed and we can conclude that this dispersion might be explained by the imposed eccentricity.

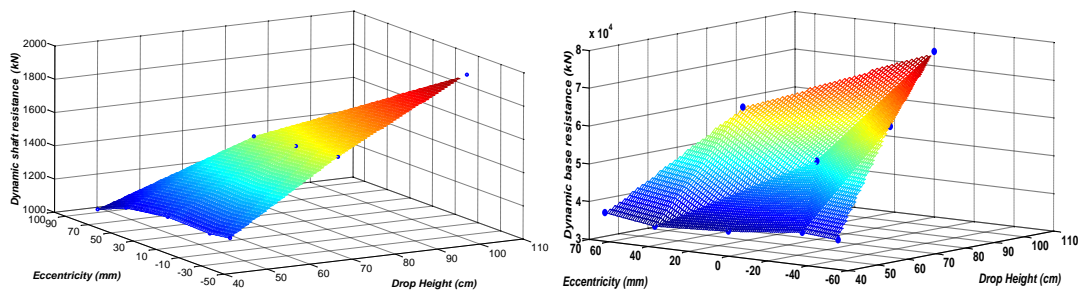


Figure 22 : (a) shaft and (b) base dynamic resistance (Tessenderlo site)

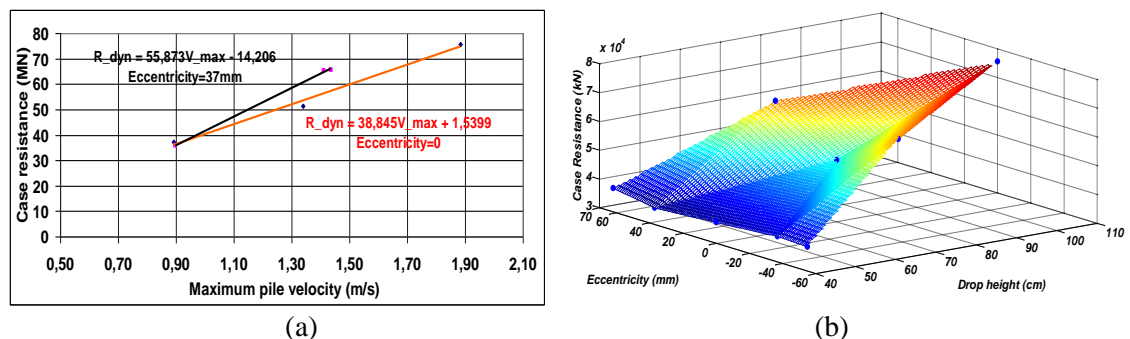


Figure 24 : Dynamic resistance in function of (a) Maximum velocity and (b) eccentricity (Tessenderlo site)

Indeed, an increase in dynamic resistance with the eccentricity especially for 70cm drop is observed. This could imply that some form of coupling may occur between axial and flexural pile response. In fact, when a pile is initially bent, horizontal pressure of the soil opposing the rotation

is changing. This means that confinement changes along the pile length depending on the pile length and the pile to soil stiffness ratio. Hence, axial shearing is affected. Numerical method of analysis must be used to accurately process the coupling between both modes of deformation.

Figure 24.a can provide some insight into the empirical Case damping factor J_c which seems to depend on the eccentricity. In fact, J_c represents the most important parameter to estimate the static bearing capacity of the pile when using the case method and it is until nowadays a difficult task to accurately estimate it. We believe that eccentricity might have a big influence on this factor and consequently static bearing capacity can be more accurately estimated.

6 CONCLUSION

Experimental data from the sites of Limelette and Tessengerlo pertaining to eccentric dynamic pile loading have been presented. Axial and flexural signal analysis was presented. Conventional axial signal analysis was first performed and 1-D formulation of the impact was used. Data show that dynamic moments can be generated during impact. Flexural energy appears to be negligible compared to the axial one but the flexure of the pile can produce a change in soil dynamic resistance. We conclude that a simple formulation should be used to model the eccentric impact together with a numerical model for coupling the analysis between axial and lateral pile responses.

REFERENCES

- Charue N. (2004), Loading rate effects on pile load-displacement behaviour derived from back calculation analysis of two load testing procedure. Ph.D in UCL.
- Goble G G., Keynote lecture: some wave mechanics applications. Application of Stress waves theory to piles (2000).
- Holeyman A. E., Keynote lecture: Technology of pile dynamics, Application of Stress waves theory to piles (2000).
- Holeyman A.E, 1988. Modelling of dynamic behaviour at the pile base. Proceedings of the 3rd International Conference on the Application of Stress-Wave Theory to Piles, Ottawa, Canada, pp. 174-185
- Holeyman. A.E (1984). Contribution à l'étude du comportement dynamique non-linéaire des pieux lors de leur battage. Ph.D dissertation ULB.
- Husein A.I.M and Ayasrah I.M (2000), Keynote lecture: Identification of soil-pile model interaction parameters from time-displacement signals. Application of Stress waves theory to piles (2000).
- Novak. M and Sheta. M (1980), Approximate approach to contact effects of piles "proc, Dynamic response of pile found: analytical aspects ASCE New York 53-79.
- Novak M., Nogami T. & Abou-ella, F., 1978. Dynamic soil reactions for plane strain case. Journal of Mechanical Engineering Div., ASCE, 104(EM4): 953-959.
- T.J. Poskitt , Keynote lecture: problems of reconciling stress wave measurements with theory application of Stress Waves theory to piles, Rotterdam, (Stress Wave1992).
- Rauche F., Keynote lecture: pile driving equipment: Capabilities and properties Application of Stress waves theory to piles (2000).
- VanAlboom, G and Whenham, V (2003). Soil investigation campaign at Limelette (Belgium) Results. In Proceeding of the Symposium on screw piles in sand. Design and recent development (2003), Swts and Zeitlinger, Eds.

ACKNOWLEDGEMENT

Special thanks go to the Oliver Tomboy and to all the technical staff of UCL who participated to the experimental campaign conducted in the Limelette site in Mai 2005

The authors also thank the BBRI for allowing access to the Limelette site, B, Pardoen and M.Bottiau (Franki) for their contribution towards Tessengerlo tests.